



## ORIGINAL ARTICLE

## Technical

## Comparative MRI Compatibility of 316L Stainless Steel Alloy and Nickel–Titanium Alloy Stents

Andrea Holton,\* Edward Walsh, Andreas Anayiotos,  
Gerald Pohost, and Ramakrishna Venugopalan

*Department of Biomedical Engineering, University of Alabama at  
Birmingham, 1075 13th Street South, Hoehn 370, Birmingham,  
AL 35294-4440*

### ABSTRACT

*The initial success of coronary stenting is leading to a proliferation in peripheral stenting. A significant portion of the stents used in a clinical setting are made of 316 low carbon stainless steel (SS). Other alloys that have been used for stent manufacture include tantalum, MP35N, and nickel–titanium (NiTi). The ferromagnetic properties of SS cause the production of artifacts in magnetic resonance imaging (MRI). The NiTi alloys, in addition to being known for their shape memory or superelastic properties, have been shown to exhibit reduced interference in MRI. Thus, the objective of this study was to determine the comparative MRI compatibility of SS and NiTi stents. Both gradient echo and spin-echo images were obtained at 1.5 and 4.1 T field strengths. The imaging of stents of identical geometry but differing compositions permitted the quantification of artifacts produced due to device composition by normalizing the radio frequency shielding effects. These images were analyzed for magnitude and spatial extent of signal loss within the lumen and outside the stent.  $B_1$  mapping was used to quantify the attenuation throughout the image. The SS stent caused significant signal loss and did not allow for visibility of the lumen. However, the NiTi stent caused only minor artifacting and even allowed for visualization of the signal from within the lumen. In addition, adjustments to the flip angle of standard imaging protocols were shown to improve the quality of signal from within the lumen.*

\*Corresponding author. Fax: (205) 975-4919; E-mail: holton@uab.edu

**Key Words:** *Magnetic resonance angiography; Stents; Artifacts; Lumen visibility*

## INTRODUCTION

The initial success of coronary stenting is leading to a proliferation in peripheral stenting. Thus, the ability to obtain improved images of the stent; the lumen, the stent–tissue interface, and the surrounding tissue could contribute to facilitating such minimally invasive interventional therapies. Nuclear magnetic resonance imaging (MRI) is a desirable alternative to invasive angiography. Cardiac MRI has been shown to provide accurate images of the proximal and medial parts of the coronary arteries.<sup>[1–3]</sup> The presence of contrast agents or anesthetics is not necessary for MRI-based angiography. Therefore, there is minimal risk of complications and MRI can assess blood flow quantitatively and qualitatively.<sup>[4]</sup> This flow information can provide important data concerning the presence of stenosis of the vessel. However, MRI does have some limitations in the presence of metallic implants.

The presence of the magnetic field can cause the implant to dislocate. This is a serious problem that can cause extensive damage to the surrounding tissues. Stouse et al. measured the deflective forces in pediatric interventional cardiology devices.<sup>[5]</sup> They found that these forces were insignificant compared to the physiological forces throughout the cardiovascular system. Scott et al. found that there was no significant deflection of any of the coronary stents in the magnetic field.<sup>[6]</sup> The second concern encountered in MRI is the production of heat from the interaction of the magnetic resonance with the implanted device. This heating can cause the necrosis of the tissue. Strohm et al. studied both the effect of heating and motion at 1.0 and 1.5 T field strengths. Their thorough study of intracoronary devices showed that neither heating nor displacement compromises the safety of patients with these implants in MR.<sup>[7]</sup> Hug et al. studied the safety and artifacting of coronary stents and showed that there were no significant heating effects caused by MR.<sup>[8]</sup> Shellock et al. evaluated the heating of heart valve prosthesis.<sup>[9]</sup> They also found an increase in temperature that was considered inconsequential from safety and biological effects standpoint. While the former limitations are not significant, the presence of metallic implants will create artifacts. An artifact can misrepresent the anatomy under study by either partially or completely voiding the desired image

space. These magnetic susceptibility artifacts are caused by local magnetic field distortion produced by the magnetic properties of the metallic device.<sup>[8]</sup> Usually, there is a good correlation between the ferromagnetic properties of a device and the size of the expected imaging artifact.<sup>[8–11]</sup> The ferromagnetic properties of alloys used in stents may lead to the production of an artifact or distortion of the imaged anatomy. A significant portion of the stents used in a clinical setting are made of 316 low carbon stainless steel (SS). The 316 SS alloy has a higher nickel content than the 304 SS that acts to stabilize the iron by forming an austenitic phase that greatly decreases the degree of ferromagnetism.<sup>[12]</sup> Although the austenitic composition or raw material is nonmagnetic, the manufacturing techniques may produce some ferromagnetic properties within the stent that can exacerbate artifacting.

The detection of stent patency and restenosis (intimal hyperplasia or plaque distribution) by magnetic resonance angiography (MRA) requires adequate visibility of the lumen. Excessive signal loss inside the stent does not allow the visualization of this information. With the use of new materials and novel designs, this signal loss can be greatly reduced. Hilfiker et al. compared stents of differing compositions and geometries using contrast-enhanced three-dimensional MRA.<sup>[13]</sup> The comparison of these stents was performed in a pulsatile flow field simulating the either femoral or external iliac arterial flow. They found that artifacting was more pronounced in SS and cobalt-based alloys and that the nitinol stents caused only minor artifacts. Klemm et al. performed extensive studies on stent compositions, orientations, and sequence types and field strengths.<sup>[4]</sup> The images were acquired with a two-dimensional gradient echo sequence using two different echo times, fast spin-echo sequences, and a three-dimensional gradient echo sequence. They found that with increased echo times the signal void became more pronounced and that the fast spin-echo sequence also decreased the visibility of the lumen. When the stent was oriented along the  $B_0$ , there was a marked reduction in artifacting in all of the gradient echo sequences. All stents oriented in the transverse direction with sagittal tomographic slices exhibited a complete signal void.

Lenhart et al. used a fast three-dimensional gradient echo sequence commonly used in contrast-enhanced

MRA studies.<sup>[14]</sup> They studied the effect of different orientations within the magnetic field. The stents were encased in a vascular phantom along the  $z$  direction, at  $45^\circ$  to the  $z$  direction, and along the  $x$  direction. They did not detect a significant change in patency or signal intensity changes within the stents along the  $z$  and  $45^\circ$  to the  $z$  direction. They did find noticeable differences comparing the  $x$  and  $z$  directions. The phase encoding and readout directions were held along the left-to-right and  $z$  direction, respectively. Along the  $z$  direction a bandlike artifact occurred at the ends of the stent, whereas along the  $x$  direction the band was not apparent and there was a narrowing of the lumen.

Bartels et al. studied the effect of radio frequency (RF) shielding in artifact production.<sup>[15]</sup> They quantified these artifacts in the form of attenuation of transmit and receive signals. Their results showed that increasing the excitation angle could improve visibility inside the device.

While all these studies explored the effect of composition and geometry on MRI, the studies were not parametric in nature, i.e., they did not control one variable and study the effect of the other exclusively. The objective of this study was to compare stents of identical geometry but different composition, specifically, 316L SS and 54/46 nickel–titanium (NiTi) alloy. Both spin- and gradient-echo images were acquired on these devices at 1.5 and 4.1 T. The variation of echo time, field of view, flip angle, and orientation within the magnet provided qualitative information concerning artifacting influencing lumen visibility. In addition,  $B_1$  mapping provided the quantification of the signal intensity throughout the device and its surroundings.

## METHODS

Generic 316L SS and 54/46 NiTi stents with internal expanded diameters of 9 mm (Fig. 1) and lengths of 23 mm were manufactured by laser cutting diamond shape apertures in tubes of raw materials (NDC:CORDIS, Fremont, CA). All samples were processed per ASTM F86 standard for surface preparation of implants.<sup>[16]</sup>

Device ferromagnetism was assessed using the method described by Hug et al.<sup>[8]</sup> The NiTi stent was suspended at its center in the test chamber that was then placed in the 4.1 T scanner. The angular position of the stent was noted prior to bringing the device into the scanner room. Angles of deflection were measured with a protractor for both vertical and longitudinal axes.

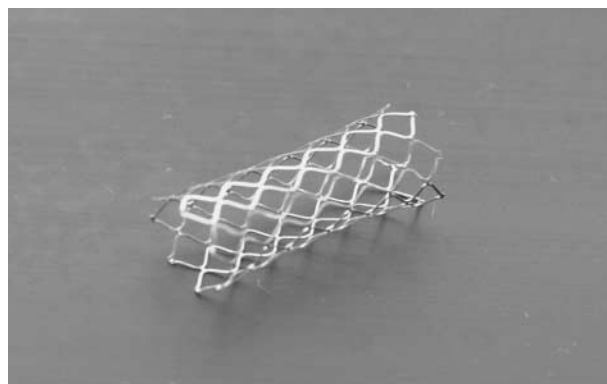


**Figure 1.** The 9-mm diameter  $\times$  23-mm length stent geometry examined in this study.

Stents were imaged at 4.1 T using a 1-m bore Oxford Scientific magnet equipped with Magnex (Oxford, England) whole body gradients and a Bruker Avance spectrometer (Billerica, MA, USA). A General Electric Signa Advantage EPI system (Waukesha, WI, USA) was used for the 1.5 T imaging. The initial study examined artifacts produced by a stent suspended in a static distilled water phantom. Paramagnetic compounds (such as  $\text{CuSO}_4$ ) normally added to phantoms to reduce the  $T_1$  of water or gel were not used in order to exclude potential chemical reaction with the samples. The 4 in. (10 cm) cubical phantom was placed laterally and longitudinally at the isocenter of the magnet thus permitting a low field of view. Images were acquired in tomographic planes corresponding to the long- and short-axis of the stents. The gradient echo images at 4.1 T were obtained using an echo time of 3.9 msec, a TR of 1000 msec, and a field of view of 12.8 cm. The gradient echo images at 1.5 T were taken using an echo time of 3.9 msec, a TR of 1000 msec, and a field of view of 12 cm. The effect of changing echo times (3.9, 5, and 8 msec) was also determined for the NiTi stents at 4.1 T. Spin-echo sequences of the NiTi stent were obtained at both 1.5 and 4.1 T with a TR of 1000 msec, and an echo time of 16 msec.

The NiTi stent was also imaged for the effect of increasing flip angles (22, 45, and  $90^\circ$ ) and orientation at 4.1 T in gradient echo sequences. Knowing the  $T_1$  of water in the test cell, and the TR of the sequence, it will be possible to quantitatively, and spatially map the actual attenuation of the  $B_1$  field within the stent and its surrounding area.<sup>[17]</sup> Thus, a  $B_1$  mapping sequence was used to quantitatively assess the RF field strength inside the NiTi stent. In this acquisition, data for two gradient echo images were acquired 20 msec apart with a

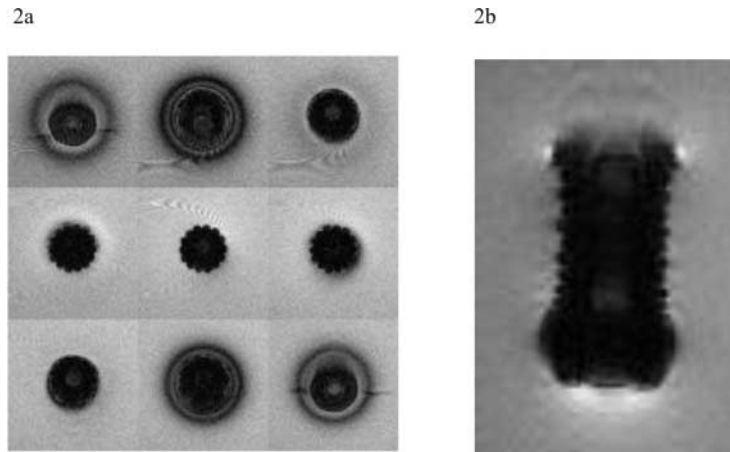


**Figure 2.** Gradient echo images of the SS stent at 4.1 T: (a) axial view and (b) sagittal view (TE of 3.9 msec, a TR of 1000 msec, and a field of view of 12.8 cm).

980 msec delay between each pair of gradient echo sequences to render the effect of longitudinal relaxation insignificant (echo time of 3.9 msec, a TR of 1000 msec, a field of view of 12.8 cm, and slice thickness of 4 mm). The flip angle on a pixel basis was calculated as:

$$\theta = \cos^{-1} \frac{I_2}{I_1}$$

where  $I_1$  and  $I_2$  are corresponding pixel intensities from the first and second image frames, respectively.

## RESULTS

The 316L stainless steel device experienced a force of  $5.2 \mu\text{N}$  at 4.1 T. There was no observable deflection for the NiTi device. Thus, tissue injury resulting from stent movement would not occur at field strengths of 4.1 T and below.

The SS device had a signal void artifact (both gradient- and spin-echo) in the short- and long-axis aspects (approximately 1.5 times the diameter and 1.25

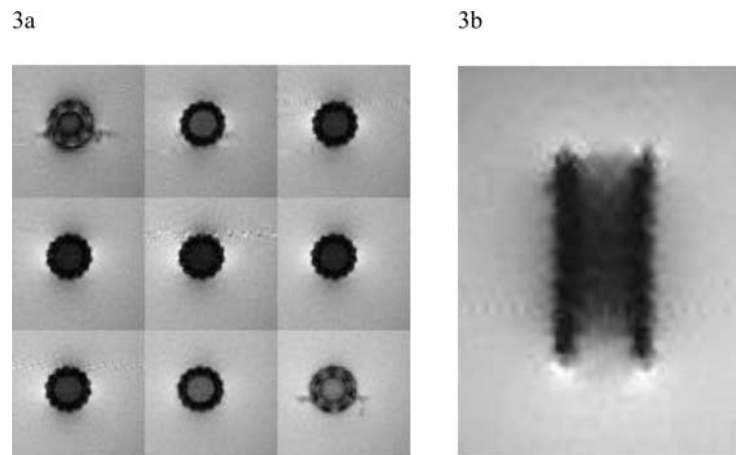


**Figure 3.** Gradient echo images of the NiTi stent at 4.1 T: (a) axial view and (b) sagittal view (TE of 3.9 msec, a TR of 1000 msec, and a field of view of 12.8 cm).

Figure a	SS (mm <sup>2</sup> )	NiTi (mm <sup>2</sup> )
upper left	321.25	48.25
upper middle	655.75	43.75
upper right	188.5	51.5
middle left	152.25	56.75
middle	141	59.5
middle right	166.75	53.75
lower left	193.75	48.5
lower middle	484.5	42.75
lower right	425	45.5

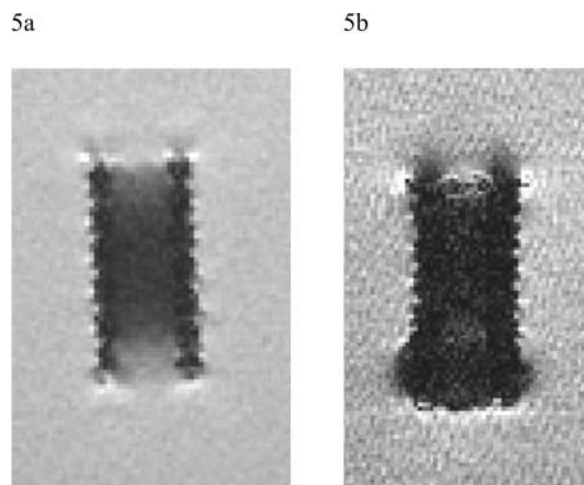
  

Figure b	547	88
----------	-----	----

**Figure 4.** Signal void areas defined as SI < 10% of peak pixel in frame.

times the length of the device) with no discernible signal from the lumen as shown in Fig. 2. For the NiTi device, no significant signal void was observed surrounding the device and a signal from the lumen was present to varying degrees depending on flip angle and stent orientation as seen in Fig. 3. The signal void areas are tabulated for Figs. 2 and 3 in Fig. 4. These effects were consistently observed at both 1.5 and 4.1 T (Fig. 5).

For the NiTi device, images were analyzed for magnitude and spatial extent of signal loss within the lumen and outside the stent. As the echo time increased (up to 8 msec), there was only a slight increase in the signal void. This is more apparent in the 4.1 T data set than in the 1.5 T data set (Fig. 6). The spin-echo sequences at both fields resulted in significantly decreased signal within the lumen compared to



**Figure 5.** Gradient echo images at 1.5 T of the (a) NiTi stent and (b) SS stent (TE of 3.9 msec, a TR of 1000 msec, and a field of view of 12 cm).

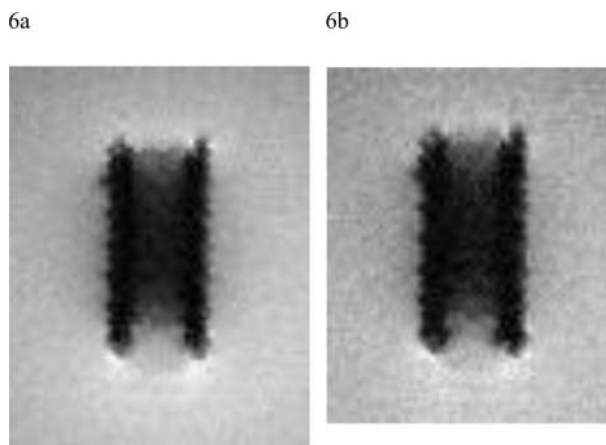


**Figure 6.** Gradient echo NiTi stent images at different echo times (TE): (a) NiTi stent image at TE = 5.0 msec and (b) NiTi stent image at TE = 8 msec (TR of 1000 msec and a field of view of 12 cm).

the gradient echo sequences, owing presumably to the need for accurate 90 and 180° flip angles (Fig. 7). Lumen visibility increased as a result of increasing the flip angle as shown in Fig. 8. The orientation of the stent relative to  $B_0$  had a slight effect on the visibility of the lumen. As shown in the  $B_1$  map in Fig. 9, it was possible to determine the achieved flip angles inside the stent for purposes of improving visibility in angiographic acquisitions (by adjustment of flip angle). As indicated in the magnitude images, there is a spatial variation of flip angles within the stent, with the minimum reached at the center of the device.

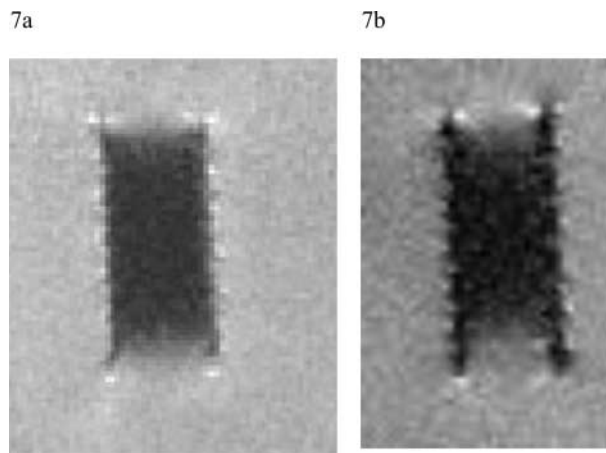


**Figure 7.** Spin-echo images of the NiTi stent at different field strengths: (a) 1.5 T and (b) 4.1 T.

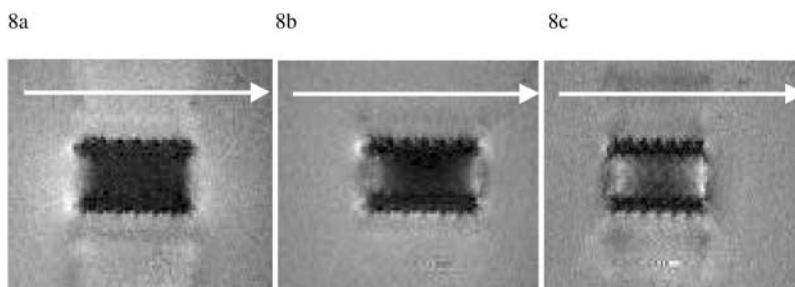


**Figure 8.** Gradient echo NiTi stent images at 4.1 T with different flip angles: (a) 22°, (b) 45°, and (c) 90°. The arrow denotes the direction of the main field ( $B_0$ ).

## DISCUSSION

The implementation of minimally or noninvasive imaging modalities continues in order to facilitate and reduce risk of complications associated with interventional therapies. Currently, the patency of a stented vessel is difficult to assess using MRA due to the incompatibility of clinically available metallic implants. In the compositional contribution of artifacting, our data indicates that the NiTi device allows for greater visualization of

the lumen and its surrounding tissue than the SS device at both mid- and high-fields. This result is important due to the increasing popularity of higher field strength (3 T) for clinical use. As our data were similar at 1.5 and 4.1 T, the compatibility of these devices at 3 T can be inferred.

The NiTi stents were far more compatible with MRI than their geometrically equivalent SS counterparts. No information concerning lumen visibility could be ascertained from the SS stent under any circumstances examined due to the compositional characteristics of this

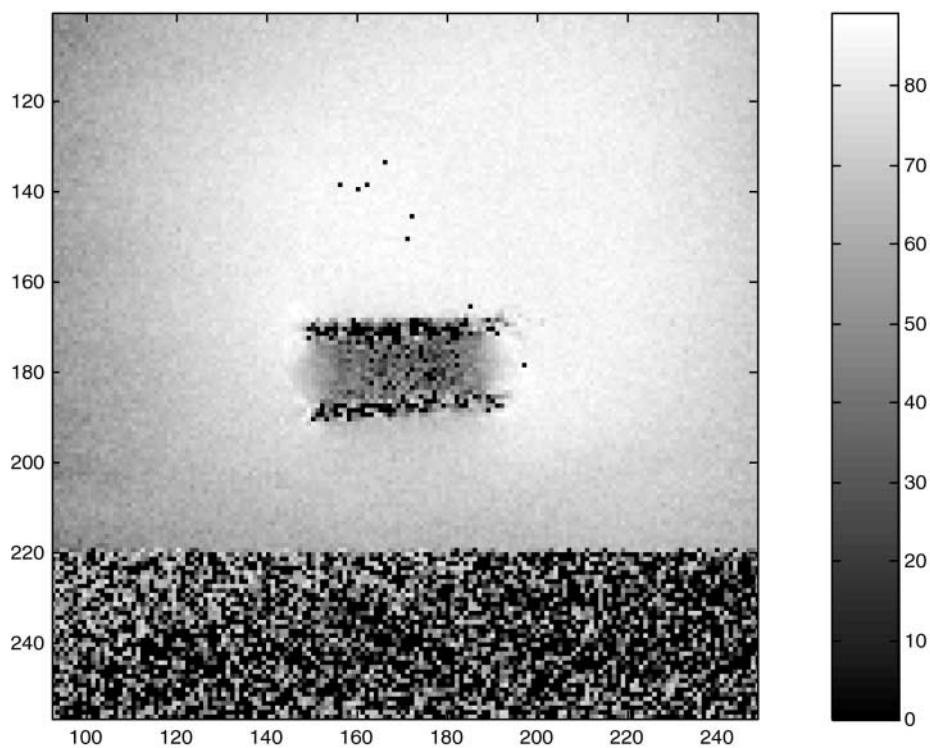


**Figure 9.** Quantitative  $B_1$  mapping of a NiTi stent image illustrating the distribution of flip angles throughout the image.

alloy. NiTi stents only contributed to minor changes in lumen visibility with variation in field strength, echo time, and orientation. While previous studies by Strohm et al., Hilfiker et al., Kelmm et al., and Lenhart et al. clearly demonstrated the improved MRI compatibility of NiTi devices, this study is unique in that it utilized a parametric approach to isolate and present only the compositional contribution to signal artifacting while normalizing the contribution from geometry-related RF shielding.

The study by Lenhart et al. simulated the clinical condition in the vasculature by situating the stents within tubing. While this approach is more representative of the flow condition in the vasculature, it may have contributed to a bandlike artifact in some of the images.

The use of spin-echo sequences is limited in the presence of metallic stents owing to the need for accurate 90 and 180° pulses. Increases in flip angle in the gradient echo sequences led to improved visibility of the lumen. The study by Bartels et al. also increased the excitation angle to increase the signal within the device under study. The quantification of the flip angles throughout the image was acquired from the  $B_1$  mapping. The flip angle within the lumen was approximated to be between 40 and 50° at a 90° setting. This information directly shows the possibility of acquiring the desired angiographic contrast needed for accurate assessment of lumen patency through determination of the  $B_1$  attenuation in the stent lumen. This attenuation value can permit the establishment of suitable flip angle settings to improve lumen visibility.

## CONCLUSION

The evaluation of lumen visibility with a variation in composition, field strength, echo time, orientation, and flip angle allowed for a thorough comparative study of the behavior of 316L SS and NiTi stents in MRI. Utilizing stents of identical geometry but differing composition allowed for normalizing any artifacts due to RF shielding and focused the study on compositional artifacting produced by the stents. It was shown that NiTi stents allowed assessment of the lumen and the surrounding area of a stent while 316L SS stents precluded the same. Further research into the relationship between stent geometry and/or composition and their resultant MRI compatibility could result in MRI-facilitated interventional therapies. In addition, MRI could be an alternative to other invasive imaging

modalities in assessing stent patency subsequent to the stenting procedure.

## REFERENCES

1. Goldfarb, J.W.; Eldelman, R.R. Coronary Arteries: Breath-Hold, Gadolinium Enhanced, and Three-Dimensional MR Angiography. *Radiology* **1998**, *206*, 830–834.
2. Pennell, D.J.; Bogren, H.G.; Keegan, J.; Firmin, D.N.; Underwood, S.R. Assessment of Coronary Artery Stenosis by Magnetic Resonance Imaging. *Heart* **1996**, *75*, 127–133.
3. Kessler, W.; Achenbach, S.; Moshage, W.; Zink, D.; Kroeker, R.; Nitz, W.; Laub, G.; Bachmann, K. Usefulness of Respiratory Gated Magnetic Resonance Coronary Angiography in Assessing Narrowings Greater or Equal to 50% in Diameter in Native Coronary Arteries and in Aortocoronary Bypass Conduits. *Am. J. Cardiol.* **1997**, *80*, 989–993.
4. Klemm, T.; Duda, S.; Machann, J.; Seekamp-Rahn, K.; Schnieder, L.; Claussen, C.D.; Schick, F. MR Imaging in the Presence of Vascular Stents: A Systematic Assessment of Artifacts for Various Stent Orientations, Sequence Types, and Field Strengths. *J. Magn. Reson. Imaging* **2000**, *12*, 606–625.
5. Stouse, P.J.; Beekeman, R.H., III. Magnetic Deflection Forces from Atrial Septal Defect and Patient Ductus Arteriosus-Occluding Device, Stents, and Coils Used in Pediatric Aged Patients. *Am. J. Cardiol.* **1996**, *78* (4), 490–491.
6. Scott, N.A.; Pettigrew, R.I. Absence of Movement of Coronary Stents After Placement in a Magnetic Resonance Imaging Field. *Am. J. Cardiol.* **1994**, *73* (12), 900–901.
7. Strohm, O.; Kivelitz, D.; Gross, W.; Schultz-Menger, J.; Liu, X.; Hamm, B.; Dietz, R.; Friedrich, M.G. Safety of Implantable Coronary Stents During 1H-Magnetic Resonance Imaging at 1.0 and 1.5 T. *J. Cardiovasc. Magn. Reson.* **1999**, *1* (3), 239–245.
8. Hug, J.; Nagel, E.; Bornstedt, A.; Schnackenburg, B.; Oswald, H.; Fleck, E. Coronary Arterial Stents: Safety and Artifacts During Magnetic Resonance Imaging. *Radiology* **2000**, *216*, 781–787.
9. Shellock, F.G.; Shellock, V.J. Metallic Stents: Evaluation of MR Imaging Safety. *Am. J. Radiol.* **1999**, *173* (3), 543–547.
10. Augustiny, N.; von Schulthess, G.K.; Meier, D.; Bosiger, P. MR Imaging of Large Nonferromagnetic Metallic Implants at 1.5 T. *J. Comput. Assist. Tomogr.* **1987**, *11* (4), 678–683.
11. Schurmann, K.; Vorwerk, D.; Buckeer, A.; Neuerburg, J.; Grosskortenhaus, S.; Haage, P.; Piroth, W.; Hunter, D.W.; Gunther, R.W. Magnetic Resonance Angiography of Nonferromagnetic Iliac Artery Stents and Stent-Grafts:



- A Comparative Study in Sheep. *Cardiovasc. Intervent. Radiol.* **1999**, *22*, 394–402.
12. Teitelbaum, G.P.; Bradley, W.G., Jr.; Klien, B.D. MR Imaging Artifacts, Ferromagnetism, and Magnetic Torque of Intravascular Filters, Stents and Coils. *Radiology* **1988**, *166*, 657–664.
  13. Hilfiker, P.R.; Quick, H.H.; Debatin, J.F. Plain and Covered Stent–Grafts: In Vitro Evaluation of Characteristics at Three-Dimensional MR Angiography. *Radiology* **1999**, *211*, 693–697.
  14. Lenhart, M.; Volk, M.; Manke, C.; Nitz, W.R.; Strotzer, M.; Feuerbach, S.; Link, J. Stent Appearance at Contrast-Enhanced MR Angiography: In Vitro Examination with 14 Stents. *Radiology* **2000**, *217*, 173–178.
  15. Bartels, L.W.; Bakker, C.J.B.; Viergever, M.A. Improved Lumen Visualization in Metallic Vascular Implants by Reducing RF Artifacts. *Magn. Reson. Med.* **2002**, *47*, 171–180.
  16. ASTM F86. Standard Practice for Surface Preparation and Marking of Metallic Surgical Implants. *Annual Book of ASTM Standards: Medical Devices and Services*; American Society for Testing and Materials: West Conshohocken, PA, 1998; Vol. 13.01, 7–9.
  17. Pan, J.W.; Twieg, D.B.; Hetherington, H.P. Quantitative Spectroscopic Imaging of the Human Brain. *Magn. Reson. Med.* **1998**, *40*, 363–369.

Received August 29, 2001

Accepted February 5, 2002